

Novel Gamma-ray Spectral Features in the Inert Doublet Model

Camilo Garcia-Cely and Alejandro Ibarra

*Physik-Department T30d, Technische Universität München,
James-Franck-Straße, 85748 Garching, Germany*

March 12, 2018

Abstract

The inert doublet model contains a neutral stable particle which is an excellent dark matter candidate. We discuss in this paper the indirect signatures of this model in gamma-rays when the dark matter mass is larger than the W boson mass. We show that, in addition to the featureless gamma-ray spectrum produced in the annihilations into two weak gauge bosons, the model generically predicts a distinctive spectral feature from the internal bremsstrahlung process $H^0 H^0 \rightarrow W^+ W^- \gamma$. We discuss under which conditions the spectral feature is generated and we construct a number of benchmark points, compatible with the observed relic density and all other direct and indirect detection experiments, which lead to a sharp gamma-ray feature from internal bremsstrahlung.

1 Introduction

The inert doublet model [1, 2, 3] is a minimal extension of the Standard Model which accounts for the dark matter of the Universe and which consists in introducing one extra scalar field, odd under an unbroken Z_2 symmetry, with identical gauge quantum number as the Standard Model Higgs. The lightest among the particles of the new sector is then stable on cosmological scales and, if electrically neutral, constitutes an excellent dark matter candidate. Indeed, it has been shown that this model can reproduce the correct dark matter relic density in a low mass regime, $10 \text{ GeV} \lesssim M_{\text{DM}} \lesssim M_W$, and a high mass regime, $M_{\text{DM}} \gtrsim 500 \text{ GeV}$, for reasonable values of the model parameters and without fine-tunings, as well as in an intermediate mass regime, $M_W \lesssim M_{\text{DM}} \lesssim 150 \text{ GeV}$, for special choices of the model parameters. However, as for all other dark matter models proposed, no signature of the inert Higgs doublet model has been observed apart from the gravitational effects of the dark matter particles in the dynamics of galaxies, clusters of galaxies or the Universe at large scale. The inert Higgs doublet model offers, however, a rich phenomenology and predicts potentially observable effects in direct and indirect dark matter searches [3, 4, 5, 6, 7, 8, 9, 10, 11, 12, 13],

collider searches [3, 14, 15, 16, 17], electroweak precision tests [3, 18] or the Higgs diphoton decay rate [19, 20, 21].

In this work we will focus in the possibility of detecting signatures of the inert Higgs doublet model through the observation of the gamma-rays which are predicted to be produced in the dark matter annihilations. More specifically, in the high mass regime, the dark matter particle annihilates mostly in the channels $H^0 H^0 \rightarrow W^+ W^-, Z^0 Z^0, hh, t\bar{t}$ while in the low mass regime, when the previous decay channels are kinematically forbidden, mostly through $H^0 H^0 \rightarrow b\bar{b}$ (three body annihilations of the type $H^0 H^0 \rightarrow WW^* \rightarrow Wf\bar{f}'$ can also be important in some regions of the parameter space [11]). The hadronization of the weak gauge bosons, Higgs boson or quarks produces neutral pions, which in turn decay into photons generating a gamma-ray flux with a featureless spectrum which could be detected at the Earth. For reasonable parameters, the gamma-ray flux from dark matter annihilations is significantly smaller than the, also featureless, diffuse galactic gamma-ray emission. Hence disentangling a dark matter signal from the astrophysical background requires a very good understanding of the latter, which is unfortunately still lacking.

A promising strategy to indirectly search for dark matter annihilations is then the search for spectral features, which might stand out over the featureless diffuse background even for moderate values of the annihilation cross section [22, 23, 24, 25, 26, 27, 28]. Furthermore, the observation of gamma-ray features in the energy spectrum would constitute a strong hint for an exotic contribution in the gamma-ray flux. It has been pointed out that the inert doublet model produces gamma-ray lines in the annihilations $H^0 H^0 \rightarrow \gamma\gamma, \gamma Z$ [6]. These processes arise at the one loop level and therefore the expected cross section is rather suppressed, $\sigma v = \mathcal{O}(10^{-28}) \text{ cm}^3 \text{ s}^{-1}$ in the low mass regime [6], which is a factor of a few below the sensitivity presently attained by the Fermi-LAT [29].

In this paper we will focus on another class of spectral features, stemming from the three body annihilation $H^0 H^0 \rightarrow W^+ W^- \gamma$. This process is generated through the exchange of a charged scalar in the t-channel and therefore produces, as discussed in [27], a bump close to the kinematical endpoint of the gamma-ray spectrum when the mass of the particle in the t-channel is degenerated to the dark matter mass. This situation naturally occurs in the high mass regime of the inert doublet model, therefore this signature is generically expected to appear. We will review in Section 2 the main features of the inert doublet dark matter model. Then, in Section 3 we will analyze the gamma-ray production via the internal bremsstrahlung and in Section 4 the possibility of detecting the associated spectral feature in gamma-ray telescopes. Lastly, we will present our conclusions in Section 5 and an Appendix containing details of the calculation of the annihilation cross section in the internal bremsstrahlung process.

2 The inert doublet Model

We consider the Inert Doublet Model (IDM), where the particle content of the Standard Model is extended by one complex scalar field η , which is a singlet under $SU(3)_C$, doublet under $SU(2)_L$ and has hypercharge 1/2. Furthermore, we postulate a discrete Z_2 symmetry

under which the Standard Model particles are even while the extra scalar η is odd. With this particle content the Lagrangian can be cast as $\mathcal{L} = \mathcal{L}_{\text{SM}} + \mathcal{L}_\eta$, where \mathcal{L}_{SM} is the Standard Model Lagrangian including a potential for the Higgs doublet Φ

$$\mathcal{L}_{\text{SM}} \supset -m_1^2 \Phi^\dagger \Phi - \lambda_1 (\Phi^\dagger \Phi)^2, \quad (1)$$

and \mathcal{L}_η is the most general Z_2 invariant Lagrangian involving the scalar doublet η

$$\begin{aligned} \mathcal{L}_\eta = & (D_\mu \eta)^\dagger (D^\mu \eta) - m_2^2 \eta^\dagger \eta - \lambda_2 (\eta^\dagger \eta)^2 - \lambda_3 (\Phi^\dagger \Phi) (\eta^\dagger \eta) \\ & - \lambda_4 (\Phi^\dagger \eta) (\eta^\dagger \Phi) - \frac{1}{2} (\lambda_5 (\Phi^\dagger \eta) (\Phi^\dagger \eta) + \text{h.c.}), \end{aligned} \quad (2)$$

where D_μ denotes the covariant derivative. Notice that all mass parameters and quartic couplings can be taken real and that CP is thus conserved. After the electroweak symmetry breaking, and assuming that the Z_2 symmetry remains unbroken, only the Higgs doublet acquires an expectation value,

$$\langle \Phi \rangle = \begin{pmatrix} 0 \\ \langle \Phi^0 \rangle \end{pmatrix}, \quad \langle \eta \rangle = \begin{pmatrix} 0 \\ 0 \end{pmatrix}, \quad (3)$$

where $\langle \Phi^0 \rangle = \sqrt{-\frac{m_1^2}{2\lambda_1}} \approx 174 \text{ GeV}$. Besides the standard model Higgs particle h , the other scalar particles from the extra doublet $\eta = \begin{pmatrix} H^+ \\ \frac{1}{\sqrt{2}}(H^0 + iA^0) \end{pmatrix}$ are two charged states H^\pm , one CP-even neutral state H^0 and one CP-odd neutral state A^0 . In terms of these fields, the scalar potential in the unitary gauge reads

$$\begin{aligned} V_{\text{Scalar}} = & \frac{1}{2} \left(M_h^2 h^2 + M_H^0 H^{02} + M_{A^0}^2 A^{02} + M_{H^\pm}^2 H^+ H^- \right) + \lambda_1 \left(\frac{1}{4} h^4 + \sqrt{2} \langle \Phi^0 \rangle h^3 \right) \\ & + \lambda_2 \left(\frac{1}{2} A^{02} + \frac{1}{2} H^{02} + H^+ H^- \right)^2 + \left(\frac{1}{2} h^2 + \sqrt{2} \langle \Phi^0 \rangle h \right) \left(\lambda_{A^0} A^{02} + \lambda_{H^0} H^{02} + \lambda_3 H^+ H^- \right), \end{aligned}$$

where

$$\begin{aligned} M_h^2 = -2m_1^2, \quad M_{H^0}^2 = m_2^2 + 2\lambda_{H^0} \langle \Phi^0 \rangle^2, \quad M_{A^0}^2 = m_2^2 + 2\lambda_{A^0} \langle \Phi^0 \rangle^2, \quad M_{H^\pm}^2 = m_2^2 + \lambda_3 \langle \Phi^0 \rangle^2, \\ \lambda_{H^0} = \frac{1}{2}(\lambda_3 + \lambda_4 + \lambda_5), \quad \lambda_{A^0} = \frac{1}{2}(\lambda_3 + \lambda_4 - \lambda_5). \end{aligned} \quad (4)$$

Due to the existence of the Z_2 symmetry, the lightest among the extra particles is stable and, if neutral, also a dark matter candidate. In fact, the role of H^0 and A^0 can be interchanged by performing $(H^0, A^0) \rightarrow (-A^0, H^0)$ and $\lambda_5 \rightarrow -\lambda_5$. We will assume in what follows, and without loss of generality, that H^0 is the dark matter candidate, which occurs, according to eq.(4), when $\lambda_5 < 0$.

The scalar potential eq.(4) is determined by seven independent parameters. Two of them are already known: they are the Higgs boson mass – which will be assumed equal to $M_h \approx 125 \text{ GeV}$ – and the vacuum expectation value of the Higgs field. These two are related

to the Lagrangian parameters m_1 and λ_1 . Among the remaining five parameters, only one is dimensionful and can be chosen to be the dark matter mass M_{H^0} . The other independent parameters can be chosen as $\lambda_2, \lambda_3, \lambda_4$ and λ_5 . Notice that the last two determine the mass splittings between the different exotic particles, concretely

$$M_{H^+}^2 = M_{H^0}^2 - (\lambda_4 + \lambda_5)\langle\Phi^0\rangle^2, \quad M_{A^0}^2 = M_{H^0}^2 - 2\lambda_5\langle\Phi^0\rangle^2. \quad (5)$$

The quartic couplings are constrained from the requirement of vacuum stability [30]

$$\lambda_1 > 0, \quad \lambda_2 > 0, \quad \lambda_3 > -2(\lambda_1\lambda_2)^{\frac{1}{2}}, \quad \lambda_3 + \lambda_4 - |\lambda_5| > -2(\lambda_1\lambda_2)^{\frac{1}{2}}. \quad (6)$$

Besides, the unitarity of the S -matrix for scalar-to-scalar scattering sets upper limits on certain combinations of couplings [31, 32]

$$\begin{aligned} \lambda_1 + \lambda_2 \pm \sqrt{(\lambda_1 - \lambda_2)^2 + \lambda_4^2} &< 8\pi, & \lambda_3 \pm \lambda_4 &< 8\pi \\ \lambda_1 + \lambda_2 \pm \sqrt{(\lambda_1 - \lambda_2)^2 + \lambda_5^2} &< 8\pi, & \lambda_3 \pm \lambda_5 &< 8\pi \\ 3(\lambda_1 + \lambda_2) \pm \sqrt{9(\lambda_1 - \lambda_2)^2 + (2\lambda_3 + \lambda_4)^2} &< 8\pi, & \lambda_3 + 2\lambda_4 \pm 3\lambda_5 &< 8\pi. \end{aligned} \quad (7)$$

Lastly, it is common to impose also perturbativity on the parameters of the model. This condition along with the vacuum stability requirement significantly constrain the mass splittings among the exotic particles. Moreover, for a heavy exotic neutral Higgs ($M_{H^0} \gg M_W$) the splitting is relatively small and we expect the particles belonging to the extra doublet to have nearly degenerate masses. This is consistent with the fact that at very high energies electroweak symmetry breaking effects are negligible and that therefore the members of any $SU(2) \times U(1)$ multiplet should have similar masses.

Many works have studied the relic abundance of H^0 [3, 4, 12, 33, 34, 35] and have shown that the measured cold dark matter abundance, $\Omega h^2 = 0.1199 \pm 0.0027$ [36] could be reproduced in three scenarios: a low mass regime $10 \text{ GeV} \lesssim M_{H^0} \lesssim M_W$, a high mass regime $M_{H^0} \gtrsim 500 \text{ GeV}$, and an intermediate mass regime $M_W \lesssim M_{H^0} \lesssim 150 \text{ GeV}$. In the low mass regime the annihilation channels into weak gauge bosons or Higgs bosons are kinematically closed and only the annihilations into light fermions, with a rate controlled by the size of the quartic couplings, are possible. The correct relic density can then be generated by adjusting the values of the quartic couplings, possibly leading to large mass splittings among the scalar mass eigenstates. For dark matter masses above the W and Z mass thresholds, the annihilations into weak gauge bosons can be very efficient in general and in fact generate a dark matter density below the measured value for $M_{H^0} \lesssim 500 \text{ GeV}$. Nevertheless, under certain circumstances, in the region $M_W \lesssim M_{H^0} \lesssim 150 \text{ GeV}$, some contributions from the annihilation diagrams cancel each other out, allowing for another viable region where it is possible to reproduce the observed relic density [12]. Lastly, when $M_{H^0} \gtrsim 500 \text{ GeV}$, following the unitarity requirement that the cross section must decrease with the inverse of $M_{H^0}^2$, the annihilation rate is again small allowing to reproduce the correct dark matter abundance.. In this case, since $M_{H^0} \gg \langle\Phi^0\rangle$, all exotic scalar states have fairly degenerate masses. In this paper we will focus in the latter case, where the dark matter particle annihilates into weak

gauge bosons via the t-channel exchange of a charged scalar which is fairly degenerate in mass with the dark matter particle. Under these conditions, it is expected an enhancement of the internal bremsstrahlung in the annihilation, which in turn might lead to an intense feature in the gamma-ray spectrum.

3 Internal bremsstrahlung in the inert doublet model

The annihilation process into W bosons with the associated emission of a photon, $H^0 H^0 \rightarrow W^+ W^- \gamma$, is described in the unitary gauge by the fourteen diagrams shown in Fig. 1. The first twelve diagrams are proportional to $g^2 e$ while the last two are proportional to $g \lambda_H e$, where g and e are, respectively, the weak and the electromagnetic coupling constants and λ_H is the quartic coupling entering in the $H^0 H^0 h$ vertex. Note that, following Eq.(4),

$$\lambda_{H^0} = \frac{1}{2} \left(\lambda_3 + \frac{M_{H^0}^2 - M_{H^+}^2}{\langle \Phi^0 \rangle^2} \right). \quad (8)$$

Then, the amplitudes of the last two diagrams depend on the quartic coupling λ_3 and on the mass splitting between the exotic charged and neutral scalars.

As discussed in detail in the Appendix, the differential velocity weighted annihilation cross section can be cast as:

$$\frac{d(\sigma v)_{W^+ W^- \gamma}}{dx} = \left. \frac{d(\sigma v)}{dx} \right|_{\text{Gauge}} + \left. \frac{d(\sigma v)}{dx} \right|_{\text{Quartic}} + \left. \frac{d(\sigma v)}{dx} \right|_{\text{Interference}}, \quad (9)$$

where each term is separately gauge invariant. In the unitary gauge, the part labelled as “gauge” receives contributions from the diagrams with a charged scalar in the t-channel and generates, in addition to the usual contribution from final state radiation, a spectral feature which is sharper when $M_{H^0} = M_{H^+}$, since in this regime the scalar propagator is enhanced for large photon energies [27]. The piece labelled as “quartic”, on the other hand, receives contributions from the diagrams with the light Higgs in the s-channel and leads to a spectrum without distinctive spectral features. Then, the shape of the differential photon spectrum from internal bremsstrahlung essentially depends on the relative weight of the gauge and the quartic contributions to the cross section, which is in turn determined by the quartic coupling λ_3 and by the mass splitting between H^0 and H^+ (the contribution labelled as “interference” can be safely neglected, as shown in the Appendix).

We show in Figure 2, upper plots, the three different contributions in Eq. (9) as a function of $x = E_\gamma/M_{H^0}$ in the limit $M_{H^0} = M_{H^+}$, which is a good approximation in the high mass regime of the inert Higgs dark matter model, for the cases $M_{H^0}=0.5$ TeV, 1 TeV and 5 TeV and for different values of the quartic coupling λ_3 . The analytic result for the differential annihilation cross section in this limit is rather complicated and is presented in the Appendix.¹ We also multiply the spectrum by x^2 to emphasize the spectral structure. The blue, green and red lines represent, respectively, the gauge, quartic and interference

¹We have used CalcHEP [37, 38] for parts of the analytical as well as for numerical computations.

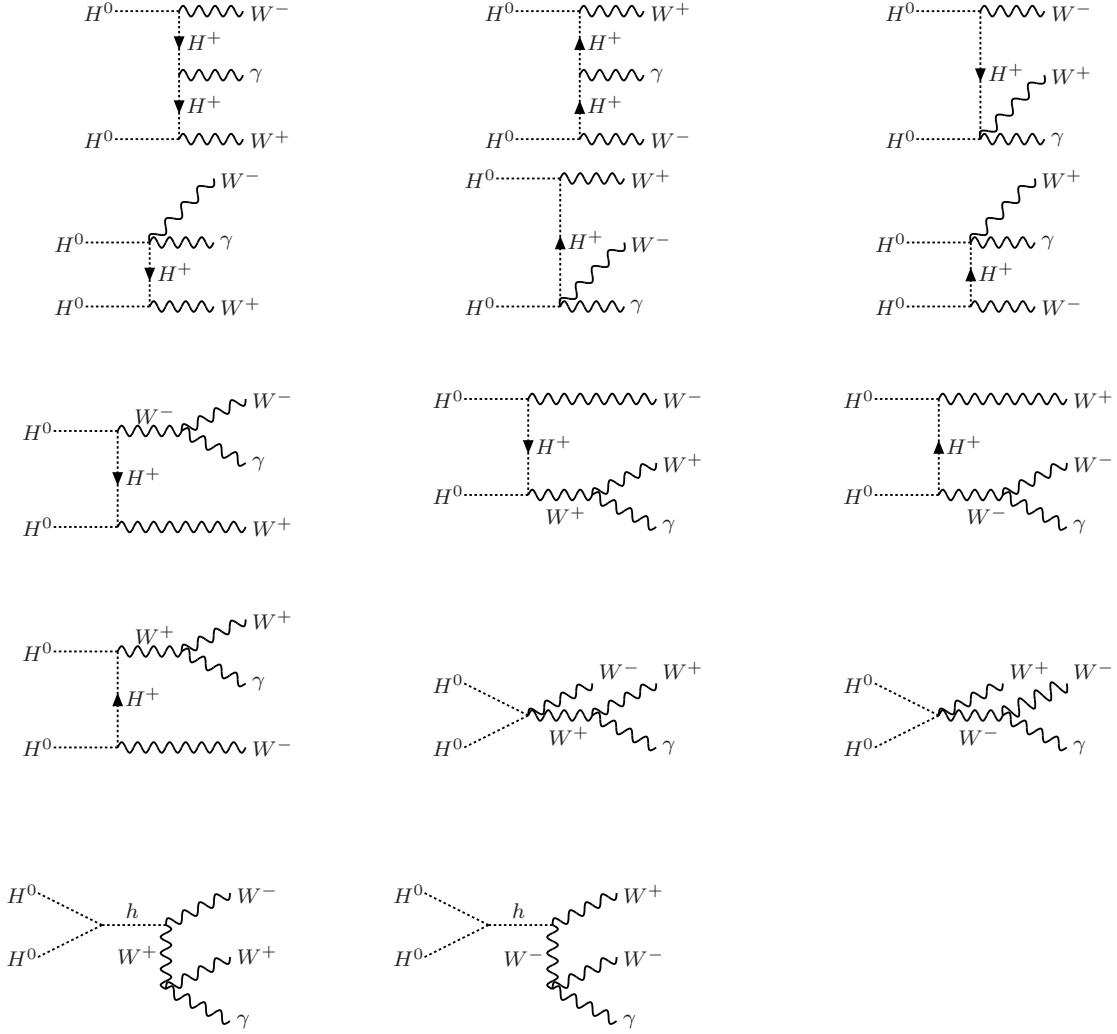


Figure 1: Feynman diagrams contributing to the annihilation process $H^0 H^0 \rightarrow W^+ W^- \gamma$ in the unitary gauge.

terms, the latter in absolute value. Besides, the darkest lines correspond to $|\lambda_3| = 0$ and the lines become lighter as $|\lambda_3|$ is increased in intervals of 0.4, the lightest lines corresponding to $|\lambda_3| = 2$. The pure gauge part produces a spectrum that depends only on the dark matter mass and that displays a feature close to the endpoint of the spectrum which becomes sharper and sharper as M_{H^0} increases. The quartic part is proportional to λ_3^2 and becomes more and more important as $|\lambda_3|$ increases, eventually dominating over the gauge part for values of x closer and closer to one. For a dark matter mass $M_{H^0} = 0.5$ TeV and $|\lambda_3| = 2$ the sharp spectral feature is practically erased in the total spectrum due to the effect of the final state radiation, however, for large dark matter masses the sharp spectral feature remains clearly visible even for $|\lambda_3| = 2$. This behaviour can be better appreciated in Fig.2, lower plots,

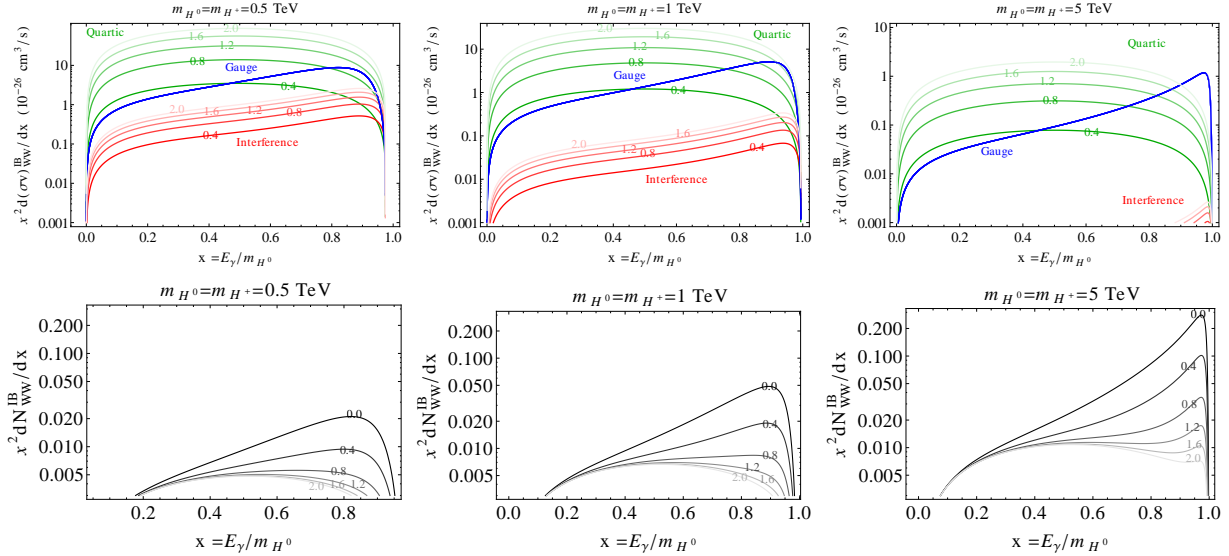


Figure 2: Contributions to the cross section (top plots) and the total multiplicity of the hard photon (bottom plots) corresponding to the internal bremsstrahlung process $H^0 H^0 \rightarrow W^+ W^- \gamma$, when the charged scalar is degenerate in mass with the dark matter particle and $m_{H^0} = 0.5$ TeV (left plots), 1 TeV (middle plots) and 5 TeV (right plots). In the top plot, the blue, green and red lines correspond, respectively, to the gauge, quartic and interference terms, the latter in absolute value. The different darknesses of the lines correspond to varying the absolute value of the quartic coupling $|\lambda_3|$ between 0 (darkest lines) and 2 (lightest lines) in intervals of 0.4 (note that for $|\lambda_3| = 0$ the quartic and interference terms vanish).

where we show the photon multiplicity from internal bremsstrahlung, defined as:

$$\frac{dN_{W^+W^-}^{\text{IB}}}{dx} = \frac{1}{(\sigma v)_{W^+W^-}} \frac{d(\sigma v)_{W^+W^- \gamma}}{dx}, \quad (10)$$

where $d(\sigma v)_{W^+W^- \gamma}/dx$ is given in Eq. (9). As before, the darkest line corresponds to $|\lambda_3| = 0$ and the lightest to $|\lambda_3| = 2$ and the intermediate lines correspond to changing λ_3 in intervals of 0.4.

For completeness, we also analyze the photon multiplicity from internal bremsstrahlung when the neutral and charged exotic Higgs particles are not degenerate in mass. The result is shown in Fig. 3, where we fixed $\lambda_3 = 0$ and we changed $\lambda_{H^0} = (\lambda_4 + \lambda_5)/2$ from 0 to -2 in intervals of -0.4 , from darkest to lightest; the mass splitting corresponding to that choice of quartic couplings can be easily derived from

$$M_{H^+}^2 - M_{H^0}^2 = -(\lambda_4 + \lambda_5) \langle \Phi^0 \rangle^2. \quad (11)$$

Remarkably, the spectrum is quite insensitive to the mass splitting, as apparent from the plot, especially for large dark matter masses. This behaviour can be understood from expanding the total amplitude squared in the mass splitting:

$$|\mathcal{M}(\lambda_3, M_{H^0}, M_{H^+})|^2 = |\mathcal{M}(\lambda_3, M_{H^0}, M_{H^0})|^2 + \mathcal{O} \left[\left(\frac{M_W^2}{M_{H^0}^2} \right) \left(\frac{M_{H^+}^2 - M_{H^0}^2}{\langle \Phi^0 \rangle^2} \right) \right]. \quad (12)$$

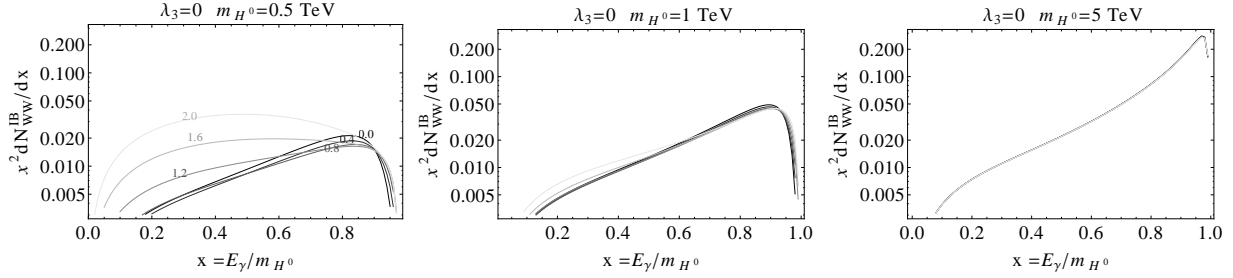


Figure 3: Total multiplicity of the hard photon produced in the internal bremsstrahlung process $H^0 H^0 \rightarrow W^+ W^- \gamma$ in the presence of a mass splitting between the dark matter mass and the charged Higgs when $m_{H^0} = 0.5$ TeV (left plot), 1 TeV (middle plot) and 5 TeV (right plot). In the plots λ_3 has been fixed to zero while $(\lambda_4 + \lambda_5)/2$, which following Eq. (11) controls the mass splitting, varies between 0 (darkest lines) and -2 (lightest lines) in intervals of 0.4.

Since $(M_{H^+}^2 - M_{H^0}^2)/\langle\Phi^0\rangle^2$ is of order one according to eq. (11), we find an additional suppression in the correction term by $M_W^2/M_{H^0}^2$. Therefore, in the limit $M_{H^0} \gg M_W$ the cross section in the non-degenerate case can be safely approximated by the cross section in the degenerate case.

4 Gamma-ray signals

To study the prospects to observe the signal from internal bremsstrahlung in gamma-ray telescopes we have constructed a series of benchmark points defined by the parameters in table 1. All these points correctly reproduce the observed cold dark matter density, as illustrated in Fig. 4, upper plot, which shows the predicted dark matter relic density for various points of the parameter space of the IDM calculated using MicrOmegas3.1 [39], working under an implementation of the inert doublet model made with FeynRules [40]. The points in cyan were generated by letting the quartic couplings vary linearly in the range $|\lambda_i| \lesssim 2$; the points in orange are the subset of those points which reproduce the correct relic density, and among them we highlight our benchmark scenarios of the table.²

The inert Higgs doublet model is subject to constraints from direct and indirect dark matter searches. Assuming that the WIMP-nucleon scattering is dominated by Higgs exchange, the spin-independent cross-section can be approximated by [3]:

$$\sigma_{H^0-p} \simeq \frac{f^2 \lambda_{H^0}^2}{\pi} \left(\frac{m_p^2}{M_{H^0} m_h^2} \right)^2 \simeq 5 \times 10^{-44} \lambda_{H^0}^2 \left(\frac{1 \text{ TeV}}{M_{H^0}} \right)^2 \text{ cm}^2 \quad (13)$$

where m_p is the nucleon mass, $f \simeq 0.3$ is the nucleonic matrix element and λ_{H^0} was defined in Eq.(4). We quote in table 2 the spin-independent WIMP-nucleon cross-sections for our

²Dark matter masses larger than 6 TeV are possible in the inert doublet model, provided $|\lambda_i| \gtrsim 2$. As discussed in Section 3, larger quartic couplings imply a larger contribution from the final state radiation to the process $H^0 H^0 \rightarrow W^+ W^- \gamma$, which erases the sharp feature. Therefore, we will restrict in this paper to $|\lambda_i| \lesssim 2$ which implies $M_{H^0} \lesssim 6$ TeV.

BMP	M_{H^0} (GeV)	M_{H^+} (GeV)	M_{A^0} (GeV)	λ_3	λ_4	λ_5	λ_{H^0}	λ_{A^0}
1	559.99	561.85	560.67	-0.02	-0.06	-0.01	-0.05	-0.03
2	983.75	993.60	991.79	0.17	-0.38	-0.26	-0.23	0.03
3	2088.3	2090.99	2100.26	0.39	0.46	-0.83	0.01	0.83
4	3596.67	3597.99	3609.7	-0.07	1.24	-1.55	-0.19	1.36
5	4212.49	4213.09	4225.29	-0.58	1.61	-1.78	-0.37	1.41
6	5382.08	5382.21	5392.59	1.08	1.82	-1.87	0.51	2.38

Table 1: Dark matter (H^0), charged Higgs (H^+) and pseudoscalar (A^0) masses, as well as the Lagrangian parameters $\lambda_{3,4,5}$ and the quartic couplings λ_{H^0} and λ_{A^0} defined in Eq. (4) for our six benchmark points.

BMP	$\sigma(H^0 p)$ (10^{-48}cm^2)	σv ($10^{-26} \text{cm}^3/\text{s}$)	BR(%)					Ωh^2
			W^+W^-	ZZ	hh	$t\bar{t}$	$W^+W^-\gamma$	
1	179.70	6.41	50.21	43.50	2.57	0.60	3.03	0.120
2	1565.57	3.95	34.87	22.84	35.97	3.03	3.17	0.122
3	0.44	4.57	13.78	84.24	0.01	0.00	1.84	0.120
4	76.09	3.52	2.36	95.23	1.83	0.01	0.51	0.119
5	215.06	3.14	8.75	83.83	5.80	0.03	1.60	0.117
6	251.71	5.38	9.29	84.92	3.92	0.01	1.86	0.111

Table 2: Scattering cross section with protons, total annihilation cross section, annihilation branching fractions and relic density in our six benchmark points.

benchmark points calculated with MicrOmegas3.1, which are, as shown in Fig. 4, bottom left plot, below the present sensitivity of the XENON100 experiment [41]; some of the points are, interestingly, within the sensitivity of the LUX [42] and XENON1T [43] experiments. We also quote in the table the annihilation cross section in the dominant $2 \rightarrow 2$ annihilation channels, $H^0 H^0 \rightarrow W^+ W^-, Z^0 Z^0, hh, t\bar{t}$, and which are safely below the limits on the cross section derived in [44] in each of these channels from the PAMELA data on the cosmic antiproton-to-proton fraction [45]. These annihilation channels are further constrained by gamma-ray observations of dwarf galaxies. The flux upper limit derived in [46] based on the joint analysis of seven Milky Way dwarfs can be translated into an approximate limit of the total annihilation cross-section $(\sigma v) \lesssim 5.0 \times 10^{-30} \text{cm}^3 \text{s}^{-1} \text{GeV}^{-2} (8\pi M_{\text{DM}}^2 / N_\gamma^{\text{tot}})$ [47], where N_γ^{tot} is the number of photons that are produced per annihilation with energies between 1 and 100 GeV and which we calculate for a given dark matter mass and annihilation channel using PYTHIA 6.4 [48]. Again, we find that all our benchmark points are below the upper limits of all the annihilation channels, as shown in Fig. 4, bottom right plot.

All these benchmark scenarios present a prominent gamma-ray feature close to the kinematic endpoint of the spectrum, as shown in Fig. 5. In fact, the appearance of such a feature is generic in the inert doublet model, as long as the relevant quartic couplings λ_3, λ_4 and λ_5 are not too large, namely not larger than 2. Under these reasonable assumptions, the dark matter particle and the charged scalar are fairly degenerate in mass. Furthermore, as argued in Section 3 it is precisely in the scenario with degenerate masses and with quartic couplings $|\lambda_i| \lesssim 2$ when a sharp spectral feature from internal bremsstrahlung is expected

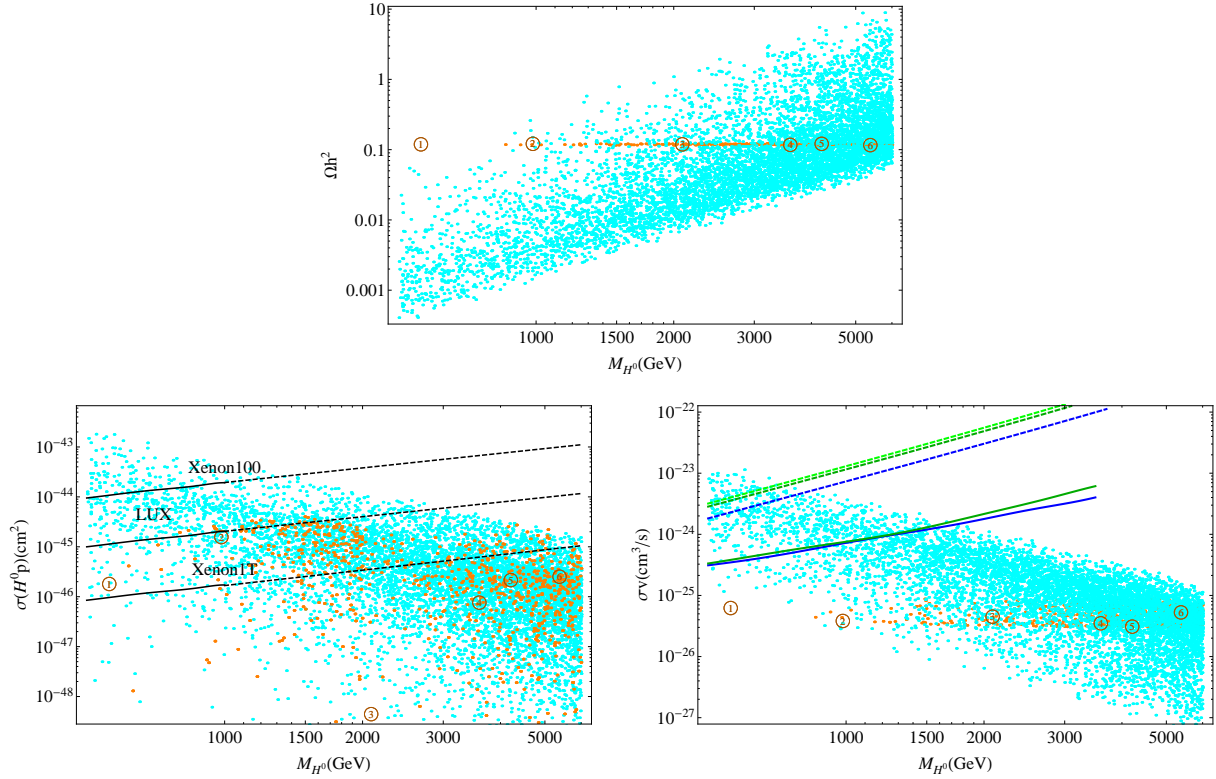


Figure 4: Relic abundance (upper plot), scattering cross section with protons (bottom left plot), and total annihilation cross section (bottom right plot) obtained from scanning the parameter space of the inert doublet model. The orange points correspond to those choices that correctly reproduce the cold dark matter relic abundance and we highlight with numbers our six benchmark points in tables 1, 2. We show, together with the predicted scattering cross sections, the limits from XENON100, as well as the projected sensitivity of XENON1T and LUX. Besides, we show together with the total annihilation cross sections the limits from dwarf galaxies (dashed lines) and antiprotons (solid lines) assuming 100% branching fraction into WW (green lines) or hh (blue lines).

to be generated.

The photon flux produced in dark matter annihilations and received at the Earth from a given solid angle in the sky, $\Delta\Omega$, is given by

$$\frac{d\phi_\gamma}{dE_\gamma} = \frac{1}{8\pi M_{H^0}^2} \sum_f (\sigma v)_f \frac{dN_\gamma^{\text{tot}}}{dE_\gamma} \frac{1}{\Delta\Omega} \int_{\Delta\Omega} J d\Omega, \quad (14)$$

where $(\sigma v)_f$ and $\frac{dN_\gamma^{\text{tot}}}{dE_\gamma}$ are, respectively, the velocity weighted annihilation cross-section and the differential energy spectrum corresponding to the annihilation channel “ f ”. Besides, the “ J -factor” is the integral of the squared dark matter density ρ_{H^0} along the line of sight, $J = \int_{\text{l.o.s.}} ds \rho_{H^0}^2$. We choose for our study the Einasto profile, favoured by recent N -body

simulations [49, 50, 51],

$$\rho_{\text{DM}}(r) \propto \exp \left[-\frac{2}{\alpha} \left(\frac{r}{r_s} \right)^\alpha \right] \quad (15)$$

with $r_s = 20$ kpc and $\alpha = 0.17$ [52, 53], as well as the Navarro-Frenk-White (NFW) profile [54, 55]:

$$\rho_{\text{DM}}(r) \propto \frac{1}{(r/r_s)[1 + (r/r_s)]^2}, \quad (16)$$

with scale radius $r_s = 21$ kpc [56], both profiles normalized to a local dark matter density $\rho_{\text{DM}}(r = 8.5 \text{ kpc}) = 0.39 \text{ GeV cm}^{-3}$ [57, 58, 59, 60]. We will compare our predicted flux to the limits recently derived by the H.E.S.S. collaboration from a search for line-like gamma-ray features in the central part of the Milky Way halo with energies between ~ 500 GeV and ~ 25 TeV [61], which adopts a complicated search region with a J -factor given by $J = 1.2 \times 10^{25} \text{ GeV}^2 \text{ cm}^{-5}$ for the Einasto profile and $J = 6.4 \times 10^{24} \text{ GeV}^2 \text{ cm}^{-5}$ for the NFW profile [62]. We show in Fig. 6 the integrated flux of the hard photon emitted in the internal bremsstrahlung process $H^0 H^0 \rightarrow W^+ W^- \gamma$ compared to the limits derived by the H.E.S.S. collaboration for the BM4 benchmark point of [27], corresponding to the neutralino annihilation $\chi^0 \chi^0 \rightarrow W^+ W^- \gamma$ [63] and which produces a similar spectrum as $H^0 H^0 \rightarrow W^+ W^- \gamma$. In the plot it was assumed the Einasto profile; the fluxes for the NFW profile are a factor of two smaller. As apparent from the plot, present instruments are not sensitive enough to observe the signal from internal bremsstrahlung of the inert doublet model, unless the annihilation signal is boosted by astrophysical or particle physics effects by a factor $\mathcal{O}(10 - 100)$. Future instruments, such as DAMPE [64], GAMMA-400 [65] or CTA [66] will, however, close in on the signal of internal bremsstrahlung from the inert doublet model.

5 Conclusions

We have shown that the spectral feature from internal bremsstrahlung naturally emerges in the high mass regime of the inert doublet model, namely when $M_{H^0} \gtrsim 500$ GeV. In this regime, the higher order annihilation $H^0 H^0 \rightarrow W^+ W^- \gamma$ generates, due to the mass degeneracy between the charged Higgs and the dark matter particle, a distinctive hardening in the gamma-ray energy spectrum which could be observed over the featureless gamma-ray background. We have also constructed a series of benchmark points, compatible with all theoretical and experimental constraints on the inert doublet model, which present an internal bremsstrahlung feature with an intensity which is one or two order of magnitude below the H.E.S.S. limits on this class of photon line-like signatures. Future searches for gamma-ray spectral features by DAMPE, GAMMA-400 or CTA will continue closing in on the parameter space of the inert doublet dark matter model.

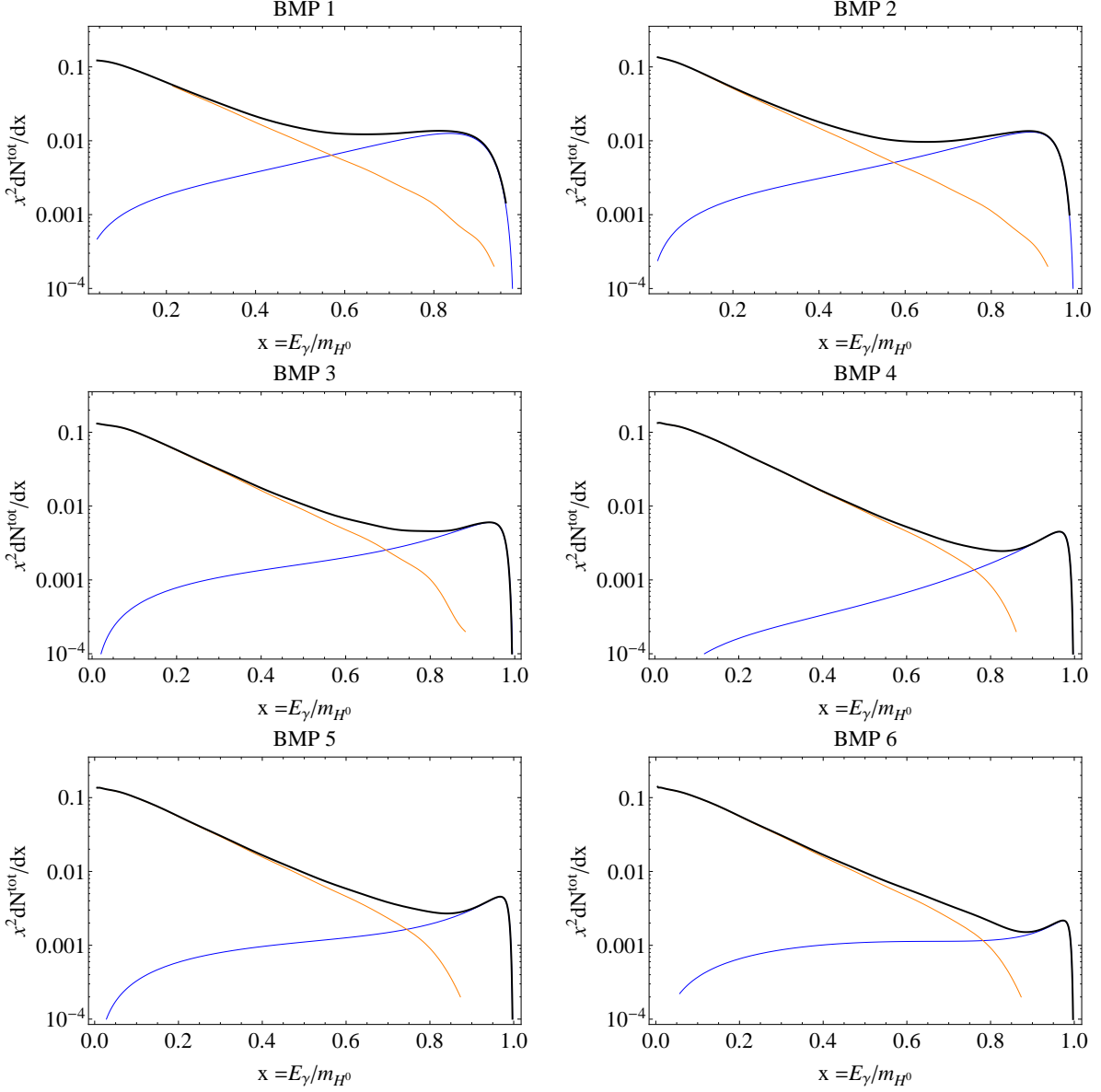


Figure 5: Predicted photon spectrum from dark matter annihilations in the inert doublet model for the six benchmark points in tables 1, 2. The red line corresponds to the photon spectrum from the $2 \rightarrow 2$ processes $H^0 H^0 \rightarrow W^+ W^-, Z^0 Z^0, hh, t\bar{t}$, following the branching fractions in tables 2, while the blue line to the $2 \rightarrow 3$ process $H^0 H^0 \rightarrow W^+ W^- \gamma$; the red line shows the total multiplicity resulting from summing up both contributions.

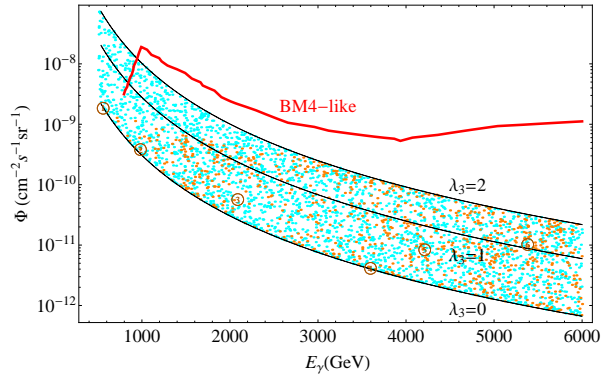


Figure 6: Same as Fig. 4, but for the integrated flux of the internal bremsstrahlung feature. We also show for reference the flux upper limit derived in [61] by the H.E.S.S. collaboration for a “BM4-like” spectral feature (red line) and the predicted flux calculated from the formulas in the Appendix for the case $M_{H^0} = M_{H^+}$ and $|\lambda_3| = 0, 1, 2$ (black lines).

Acknowledgements

We are grateful to Michael Gustafsson, Laura Lopez Honorez, Michel Tytgat and Stefan Vogl for useful discussions. This work was partially supported by the DFG cluster of excellence ‘‘Origin and Structure of the Universe’’ and by the Graduiertenkolleg ‘‘Particle Physics at the Energy Frontier of New Phenomena’’. AI thanks the Kavli Institute for Theoretical Physics in Santa Barbara, California, for hospitality during the final stages of this work.

Appendix

The differential cross-section for the process $H^0 H^0 \rightarrow W^+ W^- \gamma$ can be written as

$$d\sigma = \frac{1}{(2\pi)^5 J} |\mathcal{M}|^2 d_3(PS), \quad (17)$$

where \mathcal{M} is the scattering amplitude, J the initial flux and $d_3(PS)$ the three-body phase-space factor. These are defined by

$$J = 4E_1 E_2 v, \quad \text{where } v = \left| \frac{\vec{p}_1}{E_1} - \frac{\vec{p}_2}{E_2} \right|, \quad (18)$$

$$d_3(PS) = \delta^4(p_1 + p_2 - p_{W^+} - p_{W^-} - p_\gamma) \frac{d^3 p_{W^+}}{2E_{W^+}} \frac{d^3 p_{W^-}}{2E_{W^-}} \frac{d^3 p_\gamma}{2E_\gamma}. \quad (19)$$

Here the labelling of the momenta is self-explanatory. We are interested in the limit of zero dark matter velocity, for which $E_1, E_2 \rightarrow M_{H^0}$. Besides, the three-body phase-space factor after integration of the delta function can be written as

$$d_3(PS) = \pi^2 M_{H^0}^2 dx_+ dx, \quad \text{where } x_+ = \frac{E_{W^+}}{M_{H^0}} \text{ and } x = \frac{E_\gamma}{M_{H^0}}. \quad (20)$$

The ranges for x_+ and x are determined by the energy range of the photon and the W^+ and are given by

$$0 < x < 1 - 4\mu, \quad x_+ \leq \frac{1}{2} \left(2 - x \pm x \sqrt{1 - \frac{4\mu}{1-x}} \right) \quad (21)$$

where $\mu = \frac{M_W^2}{s} = \frac{M_W^2}{4M_{H^0}^2}$. As a result we have

$$\left. \frac{d(\sigma v)}{dx} \right|_{v \rightarrow 0} = \frac{1}{128\pi^3} \int_{x_{\min}}^{x_{\max}} |\mathcal{M}|^2 \Big|_{v \rightarrow 0} dx_+ \quad (22)$$

The diagrams that contribute to \mathcal{M} in the unitary gauge are shown in Fig. 1. The first twelve depend on M_{H^+} and M_{H^0} and are proportional to $g^2 e$, where g and e are the weak and the

electromagnetic coupling constants respectively. On the other hand, the last two diagrams depend only on M_{H^0} and are proportional to $g\lambda_H e$, where λ_H is the quartic coupling entering in the $H^0 H^0 h$ vertex. Following Eqs.(4) and (5) we can write the scattering amplitude only as a function of M_{H^0} , λ_3 , λ_4 and λ_5 . Furthermore, we notice that \mathcal{M} depends on λ_4 and λ_5 only through the combination $\lambda_4 + \lambda_5$.

In order to simplify the expression for the scattering amplitude, we find useful to write the amplitude in the following way. Since gauge transformations do not depend on the quartic couplings, \mathcal{M} can be separated in two gauge-invariant pieces

$$\mathcal{M}(M_{H^0}, \lambda_3, \lambda_4 + \lambda_5) = \mathcal{M}_{\text{Gauge}}(M_{H^0}) + \mathcal{M}_{\text{Quartic}}(M_{H^0}, \lambda_3, \lambda_4 + \lambda_5) \quad (23)$$

where the first term is the scattering amplitude when the quartic couplings are set to zero. Accordingly, the squared amplitude can be cast as

$$|\mathcal{M}|^2 = |\mathcal{M}_{\text{Gauge}}|^2 + |\mathcal{M}_{\text{Quartic}}|^2 + 2Re \left(\mathcal{M}_{\text{Gauge}} \mathcal{M}_{\text{Quartic}}^\dagger \right) \quad (24)$$

The expression for $|\mathcal{M}|^2$ is very complicated in general. However, in the limit of zero dark matter velocity, we find that

$$|\mathcal{M}(M_{H^0}, \lambda_3, \lambda_4 + \lambda_5)|^2 \Big|_{v \rightarrow 0} = |\mathcal{M}(M_{H^0}, \lambda_3, 0)|^2 \Big|_{v \rightarrow 0} + O(\mu(\lambda_4 + \lambda_5)), \quad (25)$$

since we expect μ to be very small, the dependence on $\lambda_4 + \lambda_5$ is subdominant. As a result, it is a good approximation to take $\lambda_4 + \lambda_5 \approx 0$ (or $M_{H^0} \approx M_{H^+}$), especially for dark matter masses much heavier than the W mass. Under that approximation and dropping the label $v \rightarrow 0$, we find

$$\begin{aligned} |\mathcal{M}_{\text{Gauge}}|^2 &= \frac{e^2 g^4}{2M_{H^0}^2 (x_+ - 1)^2 (x + x_+ - 1)^2 (x_+ - 2\mu)^2 (2\mu + x + x_+ - 2)^2} \\ &\left[x^6 \left(-\mu + x_+ - 1 \right) + x^5 \left(3x_+^2 + (2\mu - 9)x_+ - 4\mu^2 + 6 \right) + x^4 \left(5x_+^3 - (\mu + 20)x_+^2 \right. \right. \\ &+ 2(7\mu^2 - 6\mu + 15)x_+ - 10\mu^3 - 6\mu^2 + 11\mu - 15 \Big) + x^3 \left(5x_+^4 - (6\mu + 25)x_+^3 \right. \\ &+ 2(3\mu^2 + 6\mu + 25)x_+^2 + (40\mu^3 - 66\mu^2 + 20\mu - 50)x_+ - 4(6\mu^4 + 3\mu^3 - 12\mu^2 + 6\mu - 5) \Big) \\ &+ x^2 \left(3x_+^5 - (3\mu + 20)x_+^4 + (-16\mu^2 + 28\mu + 50)x_+^3 + (40\mu^3 + 2\mu^2 - 44\mu - 65)x_+^2 \right. \\ &+ 2(12\mu^4 - 72\mu^3 + 49\mu^2 - 2\mu + 24)x_+ - 16 - 24\mu^5 + 16\mu^4 + 78\mu^3 - 76\mu^2 + 22\mu \Big) \\ &+ x(x_+ - 1) \left(x_+^5 - 8x_+^4 + (-8\mu^2 + 8\mu + 22)x_+^3 + 4(10\mu^2 - 8\mu - 7)x_+^2 \right. \\ &+ (24\mu^4 - 64\mu^3 - 2\mu^2 + 20\mu + 20)x_+ - 4(12\mu^4 - 26\mu^3 + 14\mu^2 - 3\mu + 2) \Big) \\ &\left. - (x_+ - 1)^2 \left(x_+^4 - 4x_+^3 + (-8\mu^2 + 4\mu + 6)x_+^2 + 4(4\mu^2 - 2\mu - 1)x_+ \right. \right. \\ &\left. \left. + 24\mu^4 - 40\mu^3 + 18\mu^2 - 4\mu + 2 \right) \right], \quad (26) \end{aligned}$$

$$|\mathcal{M}_{\text{Quartic}}|^2 = \frac{e^2 \lambda_3^2}{M_{H^0}^2 (x_+ - 1)^2 (x + x_+ - 1)^2 (1 - \mu_h)^2} \left[\begin{aligned} &2\mu x^4 + 4\mu x^3 (x_+ - 1) + x^2 (4\mu x_+^2 + 12\mu^2 x_+ - 12\mu x_+ + x_+ - 12\mu^3 - 8\mu^2 + 7\mu - 1) \\ &+ x(12\mu^2 - 4\mu + 1)(x_+^2 - 3x_+ + 2) - (12\mu^2 - 4\mu + 1)(x_+ - 1)^2 \end{aligned} \right], \quad (27)$$

$$2\text{Re} \left(\mathcal{M}_{\text{Gauge}} \mathcal{M}_{\text{Quartic}}^\dagger \right) = \frac{2e^2 g^2 \mu \lambda_3}{M_{H^0}^2 (x_+ - 1)^2 (x + x_+ - 1)^2 (1 - \mu_h) (x_+ - 2\mu) (2\mu + x + x_+ - 2)} \left[\begin{aligned} &x^4 (1 - x_+) + x^3 (x_+^2 + (3 - 12\mu)x_+ + 6\mu^2 + 9\mu - 4) + x^2 (4x_+^3 - 3(4\mu + 3)x_+^2 \\ &- 6\mu(2\mu - 7)x_+ + 12\mu^3 - 27\mu + 5) + x(x_+ - 1) (2x_+^3 - 10x_+^2 + 2(-6\mu^2 + 9\mu + 4)x_+ \\ &+ 24\mu^2 - 30\mu + 3) - (x_+ - 1)^2 (-12\mu^2 + 12\mu + 2x_+^2 - 4x_+ - 1) \end{aligned} \right], \quad (28)$$

where $\mu_h = \frac{M_h^2}{s} = \frac{M_h^2}{4M_{H^0}^2}$. Notice that the interference term is proportional to μ and it is therefore subdominant. Under the same approximation, the corresponding parts of the velocity weighted cross-section are given by

$$\begin{aligned} \left. \frac{d(\sigma v)}{dx} \right|_{\text{Gauge}} &= -\frac{e^2 g^4}{128\pi^3 M_{H^0}^2 (1 - 2\mu)^3} \quad (29) \\ &\times \left[\left(\frac{2 - 4x + 6x^2 - 4x^3 + x^4 - 10\mu + 16x\mu - 20x^2\mu + 8x^3\mu + 16\mu^2 - 20x\mu^2 + 18x^2\mu^2 - 8\mu^3 + 8x\mu^3}{(2 - x - 4\mu)^2 (1 - 2x + x^2 - 4\mu + 6x\mu - x^2\mu + 4\mu^2 - 4x\mu^2)} \right. \right. \\ &+ \left. \frac{1 + x^2 - 4\mu + 6\mu^2}{x^2(1 - \mu)} \right) x(1 - x)(1 - \mu)(1 - 2\mu)A(x) \\ &+ \frac{1}{x(1 - x - 2\mu)} \left(x^4 - 2x^3(1 - 2\mu)(1 - \mu) + x^2(3 - 4\mu)(1 - 4\mu + 6\mu^2) \right. \\ &\left. - 2x(1 - 2\mu)^2(1 - 4\mu + 6\mu^2) + (1 - 2\mu)^3(1 - 4\mu + 6\mu^2) \right) B(x) \\ &+ \frac{1}{(2 - x - 4\mu)^3(1 - x - 2\mu)} \left(x^6 - 2x^5(1 - 2\mu)(4 - \mu) - 2x^4(-12 + 53\mu - 71\mu^2 + 24\mu^3) \right. \\ &- 4x^3(9 - 57\mu + 136\mu^2 - 142\mu^3 + 52\mu^4) - 2x^2(1 - 2\mu)^2(-14 + 54\mu - 87\mu^2 + 46\mu^3) \\ &\left. - 4x(-1 + 2\mu)^3(-3 + 8\mu - 13\mu^2 + 6\mu^3) + 4(1 - 2\mu)^4(1 - 2\mu + 3\mu^2) \right) C(x) \left. \right], \quad (30) \end{aligned}$$

$$\left. \frac{d(\sigma\nu)}{dx} \right|_{\text{Quartic}} = \frac{32e^2 M_{H^0}^2 \lambda_3^2}{128\pi^3 (4M_{H^0}^2 - M_h^2)^2} \times \left[-\left(\frac{1-x}{x}\right) (1-2x^2-4\mu+12\mu^2) A(x) + \left(\frac{1-x-2\mu}{x}\right) (1-4\mu+12\mu^2) B(x) \right], \quad (31)$$

$$\left. \frac{d(\sigma\nu)}{dx} \right|_{\text{Interference}} = \frac{16e^2 g^2 \lambda_3 \mu}{128\pi^3 (4M_{H^0}^2 - M_h^2)} \left[-3 \left(\frac{1-x}{x}\right) A(x) + \left(\frac{x^4 - x^3(7-13\mu) - 15x(1-2\mu)^3 + 6(1-2\mu)^4 + 2x^2(8-31\mu+30\mu^2)}{x(2-x-4\mu)(1-2\mu)(1-x-2\mu)}\right) B(x) + \left(\frac{x^3 - (1-2\mu)^2 + x^2(-3+5\mu) + x(2-6\mu+4\mu^2)}{(2-x-4\mu)(1-2\mu)(1-x-2\mu)}\right) C(x) \right], \quad (32)$$

where

$$A(x) = \sqrt{1 - \frac{4\mu}{1-x}}, \quad B(x) = \log \left[\frac{1+A(x)}{1-A(x)} \right], \quad C(x) = \log \left[\frac{2-x+A(x)x-4\mu}{2-x-A(x)x-4\mu} \right].$$

References

- [1] N. G. Deshpande and E. Ma, *Pattern of Symmetry Breaking with Two Higgs Doublets*, *Phys.Rev.* **D18** (1978) 2574.
- [2] E. Ma, *Verifiable radiative seesaw mechanism of neutrino mass and dark matter*, *Phys.Rev.* **D73** (2006) 077301, [[hep-ph/0601225](#)].
- [3] R. Barbieri, L. J. Hall, and V. S. Rychkov, *Improved naturalness with a heavy Higgs: An Alternative road to LHC physics*, *Phys.Rev.* **D74** (2006) 015007, [[hep-ph/0603188](#)].
- [4] L. Lopez Honorez, E. Nezri, J. F. Oliver, and M. H. Tytgat, *The Inert Doublet Model: An Archetype for Dark Matter*, *JCAP* **0702** (2007) 028, [[hep-ph/0612275](#)].
- [5] D. Majumdar and A. Ghosal, *Dark Matter candidate in a Heavy Higgs Model - Direct Detection Rates*, *Mod.Phys.Lett.* **A23** (2008) 2011–2022, [[hep-ph/0607067](#)].
- [6] M. Gustafsson, E. Lundstrom, L. Bergstrom, and J. Edsjo, *Significant Gamma Lines from Inert Higgs Dark Matter*, *Phys.Rev.Lett.* **99** (2007) 041301, [[astro-ph/0703512](#)].
- [7] P. Agrawal, E. M. Dolle, and C. A. Krenke, *Signals of Inert Doublet Dark Matter in Neutrino Telescopes*, *Phys.Rev.* **D79** (2009) 015015, [[arXiv:0811.1798](#)].
- [8] S. Andreas, M. H. Tytgat, and Q. Swillens, *Neutrinos from Inert Doublet Dark Matter*, *JCAP* **0904** (2009) 004, [[arXiv:0901.1750](#)].

- [9] E. Nezri, M. H. Tytgat, and G. Vertongen, *$e+$ and anti- p from inert doublet model dark matter*, *JCAP* **0904** (2009) 014, [arXiv:0901.2556].
- [10] C. Arina, F.-S. Ling, and M. H. Tytgat, *IDM and i IDM or The Inert Doublet Model and Inelastic Dark Matter*, *JCAP* **0910** (2009) 018, [arXiv:0907.0430].
- [11] L. Lopez Honorez and C. E. Yaguna, *The inert doublet model of dark matter revisited*, *JHEP* **1009** (2010) 046, [arXiv:1003.3125].
- [12] L. Lopez Honorez and C. E. Yaguna, *A new viable region of the inert doublet model*, *JCAP* **1101** (2011) 002, [arXiv:1011.1411].
- [13] M. Klasen, C. E. Yaguna, and J. D. Ruiz-Alvarez, *Electroweak corrections to the direct detection cross section of inert higgs dark matter*, arXiv:1302.1657.
- [14] Q.-H. Cao, E. Ma, and G. Rajasekaran, *Observing the Dark Scalar Doublet and its Impact on the Standard-Model Higgs Boson at Colliders*, *Phys.Rev.* **D76** (2007) 095011, [arXiv:0708.2939].
- [15] E. Lundstrom, M. Gustafsson, and J. Edsjo, *The Inert Doublet Model and LEP II Limits*, *Phys.Rev.* **D79** (2009) 035013, [arXiv:0810.3924].
- [16] E. Dolle, X. Miao, S. Su, and B. Thomas, *Dilepton Signals in the Inert Doublet Model*, *Phys.Rev.* **D81** (2010) 035003, [arXiv:0909.3094].
- [17] X. Miao, S. Su, and B. Thomas, *Trilepton Signals in the Inert Doublet Model*, *Phys.Rev.* **D82** (2010) 035009, [arXiv:1005.0090].
- [18] W. Grimus, L. Lavoura, O. Ogreid, and P. Osland, *The Oblique parameters in multi-Higgs-doublet models*, *Nucl.Phys.* **B801** (2008) 81–96, [arXiv:0802.4353].
- [19] A. Arhrib, R. Benbrik, and N. Gaur, *$H \rightarrow \gamma\gamma$ in Inert Higgs Doublet Model*, *Phys.Rev.* **D85** (2012) 095021, [arXiv:1201.2644].
- [20] B. Swiezewska and M. Krawczyk, *Diphoton rate in the Inert Doublet Model with a 125 GeV Higgs boson*, arXiv:1212.4100.
- [21] A. Goudelis, B. Herrmann, and O. Stal, *Dark matter in the Inert Doublet Model after the discovery of a Higgs-like boson at the LHC*, arXiv:1303.3010.
- [22] M. Srednicki, S. Theisen, and J. Silk, *Cosmic Quarkonium: A Probe of Dark Matter*, *Phys.Rev.Lett.* **56** (1986) 263.
- [23] S. Rudaz, *Cosmic production of quarkonium?*, *Phys.Rev.Lett.* **56** (1986) 2128.
- [24] L. Bergstrom and H. Snellman, *Observable monochromatic photons from cosmic photino annihilation*, *Phys.Rev.* **D37** (1988) 3737–3741.

- [25] L. Bergstrom, *Radiative processes in dark matter photino annihilation*, *Phys.Lett.* **B225** (1989) 372.
- [26] R. Flores, K. A. Olive, and S. Rudaz, *Radiative processes in LSP annihilation*, *Phys.Lett.* **B232** (1989) 377–382.
- [27] T. Bringmann, L. Bergstrom, and J. Edsjo, *New Gamma-Ray Contributions to Supersymmetric Dark Matter Annihilation*, *JHEP* **0801** (2008) 049, [[arXiv:0710.3169](#)].
- [28] A. Ibarra, S. Lopez Gehler, and M. Pato, *Dark matter constraints from box-shaped gamma-ray features*, *JCAP* **1207** (2012) 043, [[arXiv:1205.0007](#)].
- [29] **LAT Collaboration** Collaboration, M. Ackermann et al., *Fermi LAT Search for Dark Matter in Gamma-ray Lines and the Inclusive Photon Spectrum*, *Phys.Rev.* **D86** (2012) 022002, [[arXiv:1205.2739](#)].
- [30] J. F. Gunion and H. E. Haber, *The CP conserving two Higgs doublet model: The Approach to the decoupling limit*, *Phys.Rev.* **D67** (2003) 075019, [[hep-ph/0207010](#)].
- [31] I. F. Ginzburg and M. Krawczyk, *Symmetries of two Higgs doublet model and CP violation*, *Phys.Rev.* **D72** (2005) 115013, [[hep-ph/0408011](#)].
- [32] G. Branco, P. Ferreira, L. Lavoura, M. Rebelo, M. Sher, et al., *Theory and phenomenology of two-Higgs-doublet models*, *Phys.Rept.* **516** (2012) 1–102, [[arXiv:1106.0034](#)].
- [33] M. Cirelli, N. Fornengo, and A. Strumia, *Minimal dark matter*, *Nucl.Phys.* **B753** (2006) 178–194, [[hep-ph/0512090](#)].
- [34] T. Hambye and M. H. Tytgat, *Electroweak symmetry breaking induced by dark matter*, *Phys.Lett.* **B659** (2008) 651–655, [[arXiv:0707.0633](#)].
- [35] T. Hambye, F.-S. Ling, L. Lopez Honorez, and J. Rocher, *Scalar Multiplet Dark Matter*, *JHEP* **0907** (2009) 090, [[arXiv:0903.4010](#)].
- [36] **Planck Collaboration** Collaboration, P. Ade et al., *Planck 2013 results. XVI. Cosmological parameters*, [arXiv:1303.5076](#).
- [37] A. Pukhov, E. Boos, M. Dubinin, V. Edneral, V. Ilyin, et al., *CompHEP: A Package for evaluation of Feynman diagrams and integration over multiparticle phase space*, [hep-ph/9908288](#).
- [38] A. Pukhov, *CalcHEP 2.3: MSSM, structure functions, event generation, batchs, and generation of matrix elements for other packages*, [hep-ph/0412191](#).
- [39] G. Belanger, F. Boudjema, A. Pukhov, and A. Semenov, *micrOMEGAs3.1 : a program for calculating dark matter observables*, [arXiv:1305.0237](#).

- [40] N. D. Christensen and C. Duhr, *FeynRules - Feynman rules made easy*, *Comput.Phys.Commun.* **180** (2009) 1614–1641, [arXiv:0806.4194].
- [41] **XENON100 Collaboration** Collaboration, E. Aprile et al., *Dark Matter Results from 225 Live Days of XENON100 Data*, *Phys.Rev.Lett.* **109** (2012) 181301, [arXiv:1207.5988].
- [42] **LUX Collaboration** Collaboration, D. Akerib et al., *The Large Underground Xenon (LUX) Experiment*, *Nucl.Instrum.Meth.* **A704** (2013) 111–126, [arXiv:1211.3788].
- [43] **XENON1T collaboration** Collaboration, E. Aprile, *The XENON1T Dark Matter Search Experiment*, arXiv:1206.6288.
- [44] M. Cirelli and G. Giesen, *Antiprotons from Dark Matter: Current constraints and future sensitivities*, *JCAP* **1304** (2013) 015, [arXiv:1301.7079].
- [45] **PAMELA Collaboration** Collaboration, O. Adriani et al., *PAMELA results on the cosmic-ray antiproton flux from 60 MeV to 180 GeV in kinetic energy*, *Phys.Rev.Lett.* **105** (2010) 121101, [arXiv:1007.0821].
- [46] A. Geringer-Sameth and S. M. Koushiappas, *Exclusion of canonical WIMPs by the joint analysis of Milky Way dwarfs with Fermi*, *Phys.Rev.Lett.* **107** (2011) 241303, [arXiv:1108.2914].
- [47] T. Bringmann, X. Huang, A. Ibarra, S. Vogl, and C. Weniger, *Fermi LAT Search for Internal Bremsstrahlung Signatures from Dark Matter Annihilation*, *JCAP* **1207** (2012) 054, [arXiv:1203.1312].
- [48] T. Sjostrand, S. Mrenna, and P. Z. Skands, *PYTHIA 6.4 Physics and Manual*, *JHEP* **0605** (2006) 026, [hep-ph/0603175].
- [49] J. F. Navarro, A. Ludlow, V. Springel, J. Wang, M. Vogelsberger, et al., *The Diversity and Similarity of Cold Dark Matter Halos*, arXiv:0810.1522.
- [50] E. Hayashi and S. White, *Understanding the shape of the halo-mass and galaxy-mass cross-correlation functions*, arXiv:0709.3933.
- [51] L. Gao, J. F. Navarro, S. Cole, C. Frenk, S. D. White, et al., *The redshift dependence of the structure of massive LCDM halos*, arXiv:0711.0746.
- [52] J. F. Navarro, E. Hayashi, C. Power, A. Jenkins, C. S. Frenk, et al., *The Inner structure of Lambda-CDM halos 3: Universality and asymptotic slopes*, *Mon.Not.Roy.Astron.Soc.* **349** (2004) 1039, [astro-ph/0311231].
- [53] V. Springel, J. Wang, M. Vogelsberger, A. Ludlow, A. Jenkins, et al., *The Aquarius Project: the subhalos of galactic halos*, *Mon.Not.Roy.Astron.Soc.* **391** (2008) 1685–1711, [arXiv:0809.0898].

- [54] J. F. Navarro, C. S. Frenk, and S. D. White, *The Structure of cold dark matter halos*, *Astrophys.J.* **462** (1996) 563–575, [astro-ph/9508025].
- [55] J. F. Navarro, C. S. Frenk, and S. D. White, *A Universal density profile from hierarchical clustering*, *Astrophys.J.* **490** (1997) 493–508, [astro-ph/9611107].
- [56] L. Pieri, J. Lavalle, G. Bertone, and E. Branchini, *Implications of High-Resolution Simulations on Indirect Dark Matter Searches*, *Phys.Rev.* **D83** (2011) 023518, [arXiv:0908.0195].
- [57] R. Catena and P. Ullio, *A novel determination of the local dark matter density*, *JCAP* **1008** (2010) 004, [arXiv:0907.0018].
- [58] M. Weber and W. de Boer, *Determination of the Local Dark Matter Density in our Galaxy*, *Astron.Astrophys.* **509** (2010) A25, [arXiv:0910.4272].
- [59] P. Salucci, F. Nesti, G. Gentile, and C. Martins, *The dark matter density at the Sun’s location*, *Astron.Astrophys.* **523** (2010) A83, [arXiv:1003.3101].
- [60] M. Pato, O. Agertz, G. Bertone, B. Moore, and R. Teyssier, *Systematic uncertainties in the determination of the local dark matter density*, *Phys.Rev.* **D82** (2010) 023531, [arXiv:1006.1322].
- [61] **H.E.S.S. Collaboration** Collaboration, A. Abramowski et al., *Search for photon line-like signatures from Dark Matter annihilations with H.E.S.S.*, *Phys.Rev.Lett.* **110** (2013) 041301, [arXiv:1301.1173].
- [62] **H.E.S.S. Collaboration** Collaboration, A. Abramowski et al., *Search for a Dark Matter annihilation signal from the Galactic Center halo with H.E.S.S.*, *Phys.Rev.Lett.* **106** (2011) 161301, [arXiv:1103.3266].
- [63] L. Bergstrom, T. Bringmann, M. Eriksson, and M. Gustafsson, *Gamma rays from heavy neutralino dark matter*, *Phys.Rev.Lett.* **95** (2005) 241301, [hep-ph/0507229].
- [64] <http://dpnc.unige.ch/dampe/index.html>.
- [65] A. Galper, O. Adriani, R. Aptekar, I. Arkhangel’skaja, A. Arkhangel’skiy, et al., *Status of the GAMMA-400 Project*, *Adv.Space Res.* **51** (2013) 297–300, [arXiv:1201.2490].
- [66] **CTA Consortium** Collaboration, M. Actis et al., *Design concepts for the Cherenkov Telescope Array CTA: An advanced facility for ground-based high-energy gamma-ray astronomy*, *Exper.Astron.* **32** (2011) 193–316, [arXiv:1008.3703].